Shape-preserving storage of elegant Ince-Gaussian modes in warm atomic vapor

Zehao Shen (沈泽昊), Chengyuan Wang (王程远)*, Yun Chen (陈 云), Qifan Wu (吴启凡), Ye Yang (杨 晔), Xin Yang (杨 欣), Hong Gao (高 宏)**, and Fuli Li (李福利)

Ministry of Education Key Laboratory for Nonequilibrium Synthesis and Modulation of Condensed Matter, Shaanxi Provincial Key Laboratory of Quantum Information and Quantum Optoelectronic Devices and Shaanxi Provincial Key Laboratory of Optical Information Technology, School of Physics, Xi'an Jiaotong University, Xi'an 710049, China

*Corresponding author: wcy1992@xjtu.edu.cn

**Corresponding author: honggao@xjtu.edu.cn

Received February 4, 2023 | Accepted April 13, 2023 | Posted Online July 11, 2023

Multimode photonic quantum memory could enhance the information processing speed in a quantum repeater-based quantum network. A large obstacle that impedes the storage of the spatial multimode in a hot atomic ensemble is atomic diffusion, which severely disturbs the structure of the retrieved light field. In this paper, we demonstrate that the elegant Ince-Gaussian (eIG) mode possesses the ability to resist such diffusion. Our experimental results show that the overall structure of the eIG modes under different parameters maintains well after microseconds of storage. In contrast, the standard IG modes under the same circumstance are disrupted and become unrecognizable. Our findings could promote the construction of quantum networks based on room-temperature atoms.

Keywords: elegant Ince-Gaussian mode; hot atomic ensemble; antidiffusion.
DOI: 10.3788/COL202321.072701

1. Introduction

Efficient and reliable quantum memory is a crucial component in constructing repeater-based long-distance quantum networks and large-scale quantum computing[1–3]. Multimode photonic quantum memory has been a research interest recently since it can effectively increase the information processing speed[4–7]. Photons encoded in the spatial degree, the spectral degree, and the temporal degree or their combinations have been successfully stored in media, such as a cold atomic ensemble[8–11], a hot atomic vapor cell[12–15], and a doped solid system[6,16,17]. Among them, the hot atomic vapor has the advantage of easy implementation, low cost, and being capable of integration. Moreover, a distinctive feature of the hot atomic vapor cell is that its volume can be arbitrarily large[4], which is well suited for storing spatial multimode. However, hot atoms inside the cell have dramatic thermal motion, which causes coherent diffusion and severely disrupts the structure of the stored spatial multimode[18].

In order to attain the retrieved beams with high fidelity, researchers have proposed various schemes, such as the atomic analogue of the optical phase-shift lithography[19,20], storing the Fourier transform of the image[12], using the correlation imaging technique[21], and adjusting the angular deviation between the probe beam and the control beam[22]. Nevertheless, additional operation of the light field is required in all of these approaches, which increases the operation difficulty and system complexity.

The elegant Hermite–Gaussian (eHG) mode is a self-similar solution of the coherent diffusion equation[23], which enables it to resist motion-induced diffusion and keep its shape invariant during storage in the warm atomic vapor[24]. As another representative elegant mode, the elegant Ince-Gaussian (eIG) mode has attracted much research interest since it has an extra adjustable parameter (e.g., the ellipticity ε) and exhibits a continuous transition from the elegant Laguerre-Gaussian (eLG) mode to eHG mode as ε goes from zero to infinity[25,26]. From this perspective, the eIG mode has a larger information carrying capacity and broader application prospects in classical and quantum information processing. However, there is still no investigation on the storage of the eIG mode.

In this Letter, we experimentally study the storage performance of eIG beams with different mode parameters in a warm rubidium vapor cell. For comparison, some standard IG beams under the same conditions are also stored. The experimental results show that the eIG beams are spatially invariant to coherent diffusion while the retrieved standard beams undergo severe distortions and become unrecognizable. In the end, we conduct theoretical simulations and analyze the physical reasons behind this phenomenon.

2. Design of Experiment

2.1. Experimental setup

Our experiment is based on a Λ-type electromagnetically induced transparency (EIT) system, which consists of two ground states coupled to a common excited state of the ^{87}Rb atom, as is shown in Fig. 1(a). A 795 nm external-cavity diode laser is locked to the transition of $|5S_{1/2}, F=1\rangle \to |5P_{1/2}, F'=1\rangle$ as the probe beam (shown in Fig. 1(a) as $|1\rangle \to |3\rangle$). Simultaneously, another 795 nm laser used as the control beam resonates with the transition of $|5S_{1/2}, F=2\rangle \to |5P_{1/2}, F'=1\rangle$ ($|2\rangle \to |3\rangle$).

In the experiment, the probe beam has an intensity of 10 μW and a waist radius of 2 mm. The control beam has a stronger intensity of 16 mW and a waist of 5 mm to fully cover the probe beam. Figure 1(c) depicts the experimental setup. The incoming probe beam is first modulated into an eIG or IG mode by a spatial light modulator (SLM). It then passes through a $4f$ imaging system with two lenses of 500 mm focal length so that the specific pattern can be imaged precisely at the center of the Rb vapor cell. The cell is kept at 60°C and placed in a magnetic shielded cavity to block the stray magnetic field. The control beam, which is orthogonally polarized to the probe beam, is combined with the probe beam using a polarizing beam splitter (PBS) in front of the cell and then isolated by another PBS after passing through the cell. The second $4f$ imaging system is placed after the second PBS, ensuring that the retrieved probe beam will be captured by an intensified charge-coupled device camera (ICCD, Andor iStar 334T). Because of the limited separation ability of the PBS, a heated Rb vapor cell is put in front of the ICCD as an atomic filter for further filtering. Atoms in this cell are pumped to an energy level of $|5S_{1/2}, F=2\rangle$ by an extra laser that couples two states from $|5S_{1/2}, F=1\rangle$ to $|5P_{1/2}, F'=1\rangle$ to absorb the residual control beam. Furthermore, a phase-lock module (Vescent D2-135 Offset Phase Lock Servo) is utilized to lock the control beam to synchronize its phase with the probe beam, since the phase coherence of two beams is a prerequisite for obtaining a stable storage signal.

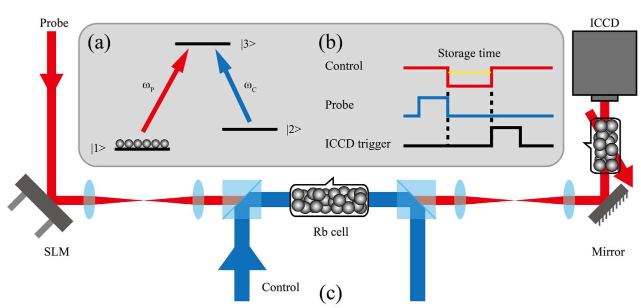

Fig. 1. (a) Energy level scheme of the ^{87}Rb D_1 transition and the transitions of the probe and the control. (b) Time sequence of the experiment. (c) Experimental setup. A probe pulse is reflected from a computer-controlled SLM with modulation into the desired modes. A $4f$ system images the SLM plane to the center of the Rb cell. Two PBSs can combine and separate the control and the probe beams. Another $4f$ system is used afterward to image the retrieved beam onto the ICCD camera. Before the beam enters the ICCD, an atomic filter is used to filter the remaining control beam.

Precise control of the sequence is also required for collecting accurate experimental data. The time sequence of the experiment is shown in Fig. 1(b). First, the control beam is opened to pump the atoms to energy level $|1\rangle$. Then, we let a 2 μs pulse of the probe beam pass through the Rb vapor cell. As soon as the probe beam enters the cell, we turn off the control beam. Then the probe beam is stored as the atomic spin wave. In the experiment, the storage time ranges from 1 μs to 4 μs. After this time interval, the control beam is turned on to release the probe beam. At the same time, we open the ICCD for 2 μs, ensuring it only collects the retrieved beam.

2.2. Expression of standard and elegant IG modes

To derive the analytical expressions of the IG modes, we let $\Psi(r)$ be the slowly varying complex envelope of a paraxial field that satisfies the paraxial wave equation (PWE), $(\nabla_t^2 + 2ik\frac{\partial}{\partial z})\Psi(r) = 0$, where ∇_t^2 is the transverse Laplacian, and k is the wave number.

The elliptic coordinates are defined as $x = f(z)\cdot\cos h\mu\cdot\cos\nu$, $y = f(z)\cdot\sin h\mu\cdot\sin\nu$, where $\mu\in[0,+\infty)$, $\nu\in[0,2\pi)$, and $f(z) = f_0\omega(z)/\omega_0$, in which f_0 is the semifocal separation with ω_0 being the beam width at the waist plane z_0. Bandres and Gutiérrez-Vega have derived the solution of IG modes[27] as

$$\begin{aligned}
\mathrm{IG}^e_{p,m}(r,\varepsilon) &= \frac{C\omega_0}{\omega(z)} C^m_p(i\mu,\varepsilon) C^m_p(\nu,\varepsilon)\exp\left[\frac{-r^2}{\omega^2(z)}\right] \\
&\quad\times\exp\left[ikz + i\frac{kr^2}{2R(z)} - i(p+1)\arctan\left(\frac{z}{z_R}\right)\right], \\
\mathrm{IG}^o_{p,m}(r,\varepsilon) &= \frac{S\omega_0}{\omega(z)} S^m_p(i\mu,\varepsilon) S^m_p(\nu,\varepsilon)\exp\left[\frac{-r^2}{\omega^2(z)}\right] \\
&\quad\times\exp\left[ikz + i\frac{kr^2}{2R(z)} - i(p+1)\arctan\left(\frac{z}{z_R}\right)\right], \qquad (1)
\end{aligned}$$

where ω_0 is the beam waist at plane $z=0$ and $\varepsilon = 2f_0^2/\omega_0^2$ is the ellipticity parameter. The superscripts of IG refer to the even (e) and odd (o) modes. C and S are normalization constants, and $z_R = k\omega_0^2/2$ is the Rayleigh range. The even and odd Ince polynomials of order p and degree m are denoted by $C^m_p(\nu,\varepsilon)$ and $S^m_p(\nu,\varepsilon)$, respectively.

When it comes to the elegant IG modes, a complex parameter $c = c(z) = k/2iq(z)$ is introduced with $q(z) = z - iz_R$. The form of the elliptic coordinates remains the same but $f(z)$ is rewritten as $f(z) = f_0/\omega_0 c(z)^{1/2}$. The general expression of the eIG beams is given by[25]

$$\mathrm{eIG}^{e}_{p,m}(r,\varepsilon) = C_e\left(\frac{q_0}{q}\right)^{\frac{p}{2}+1} C_p^m(i\mu,\varepsilon)\times C_p^m(\nu,\varepsilon)\exp(-cr^2),$$

$$\mathrm{eIG}^{o}_{p,m}(r,\varepsilon) = S_e\left(\frac{q_0}{q}\right)^{\frac{p}{2}+1} S_p^m(i\mu,\varepsilon)\times S_p^m(\nu,\varepsilon)\exp(-cr^2). \quad (2)$$

3. Experimental Result

To investigate the storage behavior of the eIG mode undergoing coherent diffusion, we modulate the probe beam into even and odd $\mathrm{eIG}_{10,2,2}$ modes, and the corresponding standard modes are also employed for comparison. The results are shown in Fig. 2. The first and third rows in Fig. 2 show the storage results of the even and odd $\mathrm{eIG}_{10,2,2}$ modes. Correspondingly, the second and fourth rows give the intensity distributions of the retrieved standard $\mathrm{IG}_{10,2,2}$ modes. The theoretical intensity distributions before storage are presented in column (1), and the images captured by the ICCD are shown in columns (2) to (5), corresponding to the original patterns and the patterns after a storage time of 1 μs to 3 μs. In the experiment, the measured storage efficiency is 15% when the storage time is 1 μs. For the eIG beams, the retrieved patterns keep their profiles intact and suffer little from atomic diffusion as the storage time increases, regardless of whether they are in the even or odd mode. However, the standard IG modes lose their internal spatial structures, and we can hardly recognize the original appearance as the storage time reaches 3 μs.

Additional experiments are carried out to explore whether the order and the ellipticity of the eIG mode would affect the fidelity of the results. We first modulate the probe beam into odd and even $\mathrm{eIG}_{20,4,2}$ modes, and the results are shown in Fig. 3. The top row presents the even modes, and the bottom row presents the odd modes. Then, we store the $\mathrm{eIG}_{20,4,\varepsilon}$ beams with ε ranging from 0 to 200. When the ellipticity comes to 0, the eIG mode converts to the eLG mode, and as ellipticity increases, it gradually converts to the eHG mode. The storage results are shown in Fig. 4. We find that the similarity and sharpness of the retrieved images do not change when the order and ellipticity vary.

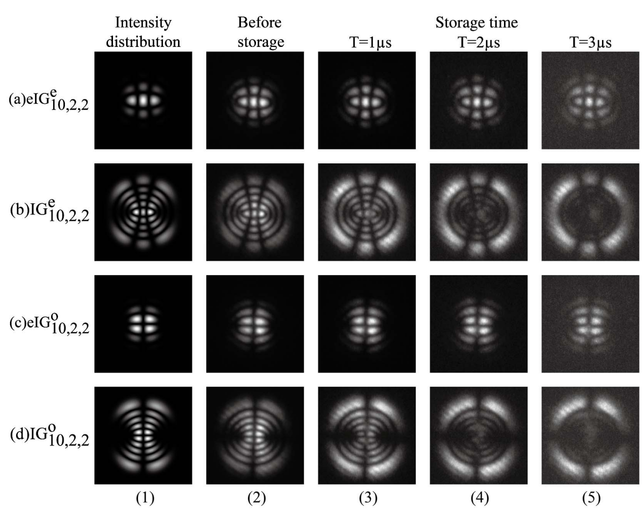

Fig. 2. Storing $\mathrm{eIG}_{10,2,2}$ and $\mathrm{IG}_{10,2,2}$ beams. Elegant beams with even modes are shown in row (a) and odd modes in row (c). Row (b) and row (d) correspond to the standard even and odd IG beams, respectively. Column (1), theoretical simulations of the original patterns. Column (2), images obtained experimentally before storage. Columns (3)–(5), images obtained after being stored for different time intervals 1 μs, 2 μs, and 3 μs, respectively.

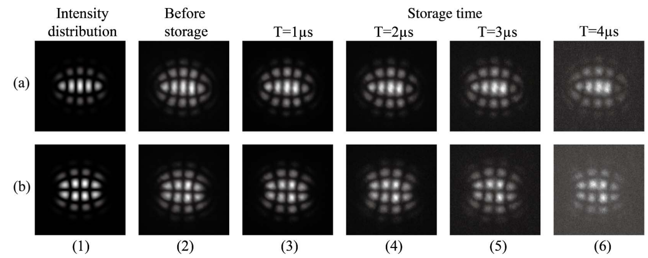

Fig. 3. Storing $\mathrm{eIG}^{e}_{20,4,2}$ mode [row (a)] and $\mathrm{eIG}^{o}_{20,4,2}$ mode [row (b)]. Same as Fig. 2, columns (1) and (2) are theoretical simulations and experimentally obtained images before storage, and columns (3)–(6) are retrieved results with storage time increasing from 1 μs to 4 μs.

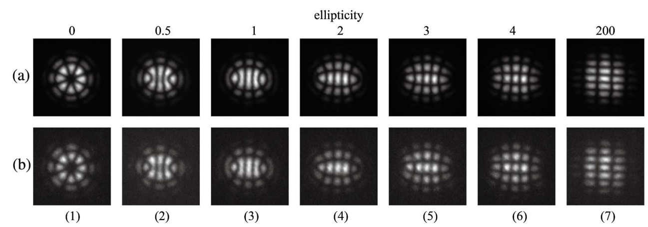

Fig. 4. Storing $\mathrm{eIG}^{e}_{20,4,\varepsilon}$ modes with ε being 0, 0.5, 1, 2, 3, 4, and 200 [column (1) to column (7)]. Row (a) shows obtained images before storage. Row (b) shows retrieved modes after a storage time of 3 μs.

4. Analysis and Discussion

From all these results, it is clearly seen that the eIG mode is robust to atomic diffusion. For quantitative analysis, we use the Pearson correlation coefficient (PCC) as a statistical tool to judge the relevance between the retrieved images and the original images[28,29]. PCC is widely used in measuring the correlation between two images. Its expression is

$$\mathrm{PCC} = \frac{\sum_{i=1}^{g}\sum_{j=1}^{h}(A_{i,j}-\bar{A})(B_{i,j}-\bar{B})}{\sqrt{\sum_{i=1}^{g}\sum_{j=1}^{h}(A_{i,j}-\bar{A})^2}\sqrt{\sum_{i=1}^{g}\sum_{j=1}^{h}(B_{i,j}-\bar{B})^2}}, \quad (3)$$

where $A_{i,j}$ and $B_{i,j}$ correspond to the grayscale value of every pixel of the image before storage and after storage, respectively. $\bar{A}$ and $\bar{B}$ are the average grayscale value of all pixels in these two images, and g and h are the number of pixels in every row and column. Since the PCC itself is normalized, its value ranges from −1 to 1. PCC = 1 means the two images have a perfectly linear correlation, while PCC = −1 indicates an anti-correlation, and two unrelated images will lead to a PCC value close to 0.

We calculate the PCC values of every mode in Figs. 1 and 2, and the results are shown in Fig. 5. As the storage time increases, the PCC values of all modes decrease. However, whether in odd or even mode, the PCC values of the elegant beams, $\mathrm{eIG}_{10,2,2}$ and $\mathrm{eIG}_{20,4,2}$, remain above 0.9 after 3 μs of storage, which illustrates that they preserve their intensity distributions quite well. Regarding the standard IG modes, the PCC values drop below 0.3 after a storage time of 3 μs, indicating that the information carried by the original modes basically disappears.

The calculation results of the PCC value further illustrate that the eIG mode is invariant to coherent diffusion. In order to analyze this phenomenon, we adopt the theory proposed by Shuker *et al.*[18,19]. Based on this theory, the retrieved beam $E(r,t+\tau)$ has been stored as

$$|E(r,t+\tau)|^2 \propto \left|\int \mathrm{d}^2 r' E(r',t) e^{-|r-r'|^2}\right|^2, \tag{4}$$

where $E(r',t)$ is the probe field and convolves with a Gaussian function $\exp^{-|r-r'|^2}$. According to the convolution theorem, we can rewrite Eq. (4) as

$$|E(r,t+\tau)|^2 \propto |\mathcal{F}^{-1}\{\mathcal{F}[E(r,t)]\cdot\mathcal{F}(e^{-|r|^2})\}|^2, \tag{5}$$

where $\mathcal{F}$ represents the Fourier transform, and $\mathcal{F}^{-1}$ represents the inverse Fourier transform. $\mathcal{F}(e^{-|r|^2})$ remains as a Gaussian function, which acts as a low-pass filter, filtering out most of the high-frequency components of the probe beam in the frequency domain.

The distribution of probe field in the spatial and frequency domains is shown in Fig. 6. The first and third rows present $\mathrm{eIG}_{10,2,2}$ modes, while the second and fourth rows are the standard IG modes for comparison. The Gaussian function $\mathcal{F}(e^{-|r|^2})$ decreases in value from the center to the edge, resulting in better preservation of the low-frequency components of the probe beam which are at the center of the frequency domain. However, the high-frequency components at the periphery of the frequency domain are greatly reduced when multiplied by $\mathcal{F}(e^{-|r|^2})$. From the second column of Fig. 6, we can find that the standard IG mode has a wide range of angular spectra in the frequency domain. Once it is Gaussian modulated by $\mathcal{F}(e^{-|r|^2})$, its high-frequency components are filtered, resulting in the loss of light field information after storage. In comparison, the distribution of the elegant modes in the frequency domain is more concentrated and is symmetrically centered about the origin of the coordinates, which means that its angular spectrum only undergoes a uniform attenuation and maintains the overall structure unchanged. Therefore, the frequency domain distribution of the retrieved beam is well preserved. So the corresponding spatial patterns are well preserved as a result. Furthermore, by upgrading the Rb cell to a paraffin-coated cell filled with inert gas and by using a combination of probes and control beams with Zeeman coherence $\Delta m = 1$[30], longer storage time of the eIG mode can potentially be achieved, potentially extending into the millisecond range.

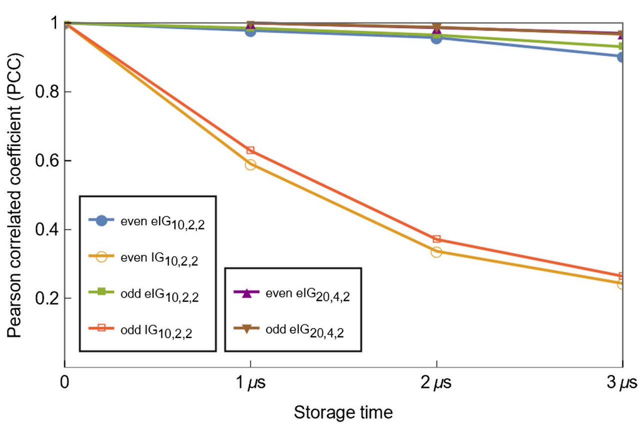

Fig. 5. Pearson correlated coefficient (PCC) values of the even $\mathrm{eIG}_{10,2,2}$ modes (with solid circles), the even $\mathrm{IG}_{10,2,2}$ modes (with hollow circles), the odd $\mathrm{eIG}_{10,2,2}$ modes (with solid squares), the odd $\mathrm{IG}_{10,2,2}$ modes (with hollow squares), the even $\mathrm{eIG}_{20,4,2}$ modes (with triangles), and the odd $\mathrm{eIG}_{20,4,2}$ modes (with inverse triangles) with storage times increasing from 1 μs to 3 μs.

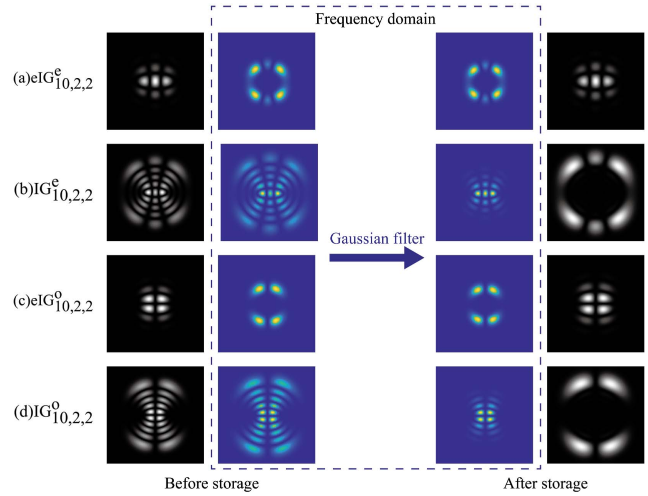

Fig. 6. Schematic diagrams illustrating the principle of the anti-diffusion mechanism of the eIG mode. Intensity distributions of the eIG and the IG modes in the spatial domain before storage [column (1)] and after storage [column (4)], and distributions in the frequency domain before storage [column (2)] and after storage, which is Gaussian filtered [column (3)]. Row (a) $\mathrm{eIG}^e_{10,2,2}$. Row (b) $\mathrm{IG}^e_{10,2,2}$. Row (c) $\mathrm{eIG}^o_{10,2,2}$. Row (d) $\mathrm{IG}^o_{10,2,2}$.

5. Conclusion

To summarize, we have studied the storage performance of eIG modes in a warm Rb vapor cell. We record the retrieved patterns of $\mathrm{eIG}_{10,2,2}$ and $\mathrm{eIG}_{20,4,2}$ modes after storage times of 1, 2, and 3 microseconds; quantify their fidelity using PCC values; and compare their storage performance to the $\mathrm{IG}_{10,2,2}$ modes. The experiment results show that after storing for 3 μs, PCC values of all elegant modes are higher than 0.9, while the values of the standard modes are less than 0.3. Moreover, eIG beams with different ellipticity are stored for 3 μs, which is found to have little effect on the storage results. Our demonstrations indicate that the eIG modes could be faithfully stored in room temperature atoms, which is helpful for building a high-dimensional and multiplexed quantum repeater. By combining it with a fiber network[31], high-fidelity and long-distance quantum communication is expected to be achievable in the future.

Acknowledgement

This work was supported by the National Natural Science Foundation of China (NSFC) (Nos. 12104358, 11774286, and 92050103).

References

1. H. J. Kimble, "The quantum internet," Nature **453**, 1023 (2008).
2. P. Kok, W. J. Munro, K. Nemoto, T. C. Ralph, J. P. Dowling, and G. J. Milburn, "Linear optical quantum computing with photonic qubits," Rev. Mod. Phys. **79**, 135 (2007).
3. N. Sangouard, C. Simon, H. De Riedmatten, and N. Gisin, "Quantum repeaters based on atomic ensembles and linear optics," Rev. Mod. Phys. **83**, 33 (2011).
4. A. Grodecka-Grad, E. Zeuthen, and A. S. Sørensen, "High-capacity spatial multimode quantum memories based on atomic ensembles," Phys. Rev. Lett. **109**, 133601 (2012).
5. C. Wang, Y. Yu, Y. Chen, M. Cao, J. Wang, X. Yang, S. Qiu, D. Wei, H. Gao, and F. Li, "Efficient quantum memory of orbital angular momentum qubits in cold atoms," Quantum Sci. Technol. **6**, 045008 (2021).
6. T.-S. Yang, Z.-Q. Zhou, Y.-L. Hua, X. Liu, Z.-F. Li, P.-Y. Li, Y. Ma, C. Liu, P.-J. Liang, X. Li, Y.-X. Xiao, J. Hu, C.-F. Li, and G.-C. Guo, "Multiplexed storage and real-time manipulation based on a multiple degree-of-freedom quantum memory," Nat. Commun. **9**, 3407 (2018).
7. Y.-H. Ye, L. Zeng, M.-X. Dong, W.-H. Zhang, E.-Z. Li, D.-C. Li, G.-C. Guo, D.-S. Ding, and B.-S. Shi, "Long-lived memory for orbital angular momentum quantum states," Phys. Rev. Lett. **129**, 193601 (2022).
8. D.-S. Ding, Z.-Y. Zhou, B.-S. Shi, and G.-C. Guo, "Single-photon-level quantum image memory based on cold atomic ensembles," Nat. Commun. **4**, 2527 (2013).
9. V. Parigi, V. D'Ambrosio, C. Arnold, L. Marrucci, F. Sciarrino, and J. Laurat, "Storage and retrieval of vector beams of light in a multiple-degree-of-freedom quantum memory," Nat. Commun. **6**, 7706 (2015).
10. D.-S. Ding, W. Zhang, Z.-Y. Zhou, S. Shi, G.-Y. Xiang, X.-S. Wang, Y.-K. Jiang, B.-S. Shi, and G.-C. Guo, "Quantum storage of orbital angular momentum entanglement in an atomic ensemble," Phys. Rev. Lett. **114**, 050502 (2015).
11. L. Zeng, Y.-H. Ye, M.-X. Dong, W.-H. Zhang, E.-Z. Li, D.-C. Li, D.-S. Ding, and B.-S. Shi, "Optical memory for arbitrary perfect Poincaré states in an atomic ensemble," Opt. Lett. **48**, 477 (2023).
12. P. K. Vudyasetu, R. M. Camacho, and J. C. Howell, "Storage and retrieval of multimode transverse images in hot atomic rubidium vapor," Phys. Rev. Lett. **100**, 123903 (2008).
13. Y.-H. Ye, M.-X. Dong, Y.-C. Yu, D.-S. Ding, and B.-S. Shi, "Experimental realization of optical storage of vector beams of light in warm atomic vapor," Opt. Lett. **44**, 1528 (2019).
14. Y. Yu, Y. Chen, C. Wang, J. Wang, Z. Sun, M. Cao, H. Gao, and F. Li, "Optical storage of Ince-Gaussian modes in warm atomic vapor," Opt. Lett. **46**, 1021 (2021).
15. S. Ming, J. Guo, Y. Wu, G. Bao, S. Wu, M. Shi, L. Chen, and W. Zhang, "Optimizing Raman quantum memory with dynamic phase," Sci. China Inf. Sci. **66**, 180505 (2023).
16. A. Seri, D. Lago-Rivera, A. Lenhard, G. Corrielli, R. Osellame, M. Mazzera, and H. de Riedmatten, "Quantum storage of frequency-multiplexed heralded single photons," Phys. Rev. Lett. **123**, 080502 (2019).
17. J.-S. Tang, Z.-Q. Zhou, Y.-T. Wang, Y.-L. Li, X. Liu, Y.-L. Hua, Y. Zou, S. Wang, D.-Y. He, G. Chen, Y.-N. Sun, Y. Yu, M.-F. Li, G.-W. Zha, H.-Q. Ni, Z.-C. Niu, C.-F. Li, and G.-C. Guo, "Storage of multiple single-photon pulses emitted from a quantum dot in a solid-state quantum memory," Nat. Commun. **6**, 8652 (2015).
18. O. Firstenberg, M. Shuker, R. Pugatch, D. R. Fredkin, N. Davidson, and A. Ron, "Theory of thermal motion in electro-magnetically induced transparency: effects of diffusion, Doppler broadening, and Dicke and Ramsey narrowing," Phys. Rev. A **77**, 043830 (2008).
19. M. Shuker, O. Firstenberg, R. Pugatch, A. Ron, and N. Davidson, "Storing images in warm atomic vapor," Phys. Rev. Lett. **100**, 223601 (2008).
20. Y. Chen, C.-Y. Wang, Y. Yu, Z.-B. Jiang, J.-W. Wang, S.-P. Zhao, D. Wei, H. Gao, and F.-L. Li, "Genetic algorithm optimization for storing arbitrary multimode transverse images in thermal atomic vapor," Appl. Phys. Lett. **118**, 234001 (2021).
21. Y.-W. Cho, J.-E. Oh, and Y.-H. Kim, "Diffusion-free image storage in hot atomic vapor," Phys. Rev. A **86**, 013844 (2012).
22. Y. Chen, C.-Y. Wang, Z.-B. Jiang, W. Zhang, Z.-H. Shen, H. Gao, and F.-L. Li, "Angular dependence of spatial frequency modulation in diffusion media," Phys. Rev. A **106**, 013704 (2022).
23. O. Firstenberg, P. London, D. Yankelev, R. Pugatch, M. Shuker, and N. Davidson, "Self-similar modes of coherent diffusion," Phys. Rev. Lett. **105**, 183602 (2010).
24. D. Yankelev, O. Firstenberg, M. Shuker, and N. Davidson, "Shape-preserving diffusion of a high-order mode," Opt. Lett. **38**, 1203 (2013).
25. M. A. Bandres, "Elegant Ince-Gaussian beams," Opt. Lett. **29**, 1724 (2004).
26. D.-M. Deng and Q. Guo, "Propagation of elliptic-Gaussian beams in strongly nonlocal nonlinear media," Phys. Rev. E **84**, 046604 (2011).
27. M. A. Bandres and J. C. Gutiérrez-Vega, "Ince-Gaussian beams," Opt. Lett. **29**, 144 (2004).
28. K. Pearson, "VII. Mathematical contributions to the theory of evolution. iii. Regression, heredity, and panmixia," Philos. Trans. R. Soc. A **187**, 253 (1896).
29. S. Mohapatra and J. C. Weisshaar, "Modified Pearson correlation coefficient for two-color imaging in spherocylindrical cells," BMC Bioinf. **19**, 428 (2018).
30. O. Katz and O. Firstenberg, "Light storage for one second at room-temperature alkali vapor," Nat. Commun. **9**, 2074 (2018).
31. Y. Zhou, B. Braverman, A. Fyffe, R. Zhang, J. Zhao, A. E. Willner, Z. Shi, and R. W. Boyd, "High-fidelity spatial mode transmission through a 1-km-long multimode fiber via vectorial time reversal," Nat. Commun. **12**, 1866 (2021).